Results in Nonlinear Analysis 8 (2025) No. 4, 109–127
https://doi.org/10.31838/rna/2025.08.04.009
Available online at www.nonlinear-analysis.com

Results in Nonlinear Analysis
ISSN 2636-7556

Peer Reviewed Scientific Journal

New optimized meshless block method for solving Time-dependent PDEs

Bilal Charmouti[1,*], Nazihah Ahmad[1], Kamarun Hizam Mansor[1]

[1]School Of Quantitative Sciences, UUM College of Arts & Sciences, Universiti Utara Malaysia, 06010 Sintok, Kedah Darul Aman, Malaysia.

Abstract

Partial differential equations (PDEs) provide mathematical models to describe real phenomena such as heat conduction, wave propagation, and many other scientific disciplines. A vast array of methods has been used to solve PDEs. Among them, multistep block methods, along with mesh-based techniques, have been utilized to discretize the time variables and the partial derivatives with respect to the spatial variable in the PDE. However, this approach encounters challenges such as discontinuities, high computational cost, and time demands. In this context, the current work proposes an Optimized Meshless Block Method (OMBM) for solving time-dependent PDEs. The method integrates Radial Basis Function–Finite Difference (RBF-FD) method for spatial discretization with a two-step hybrid block method for time integration. This combination leverages the accuracy and stability of block methods, along with the geometric flexibility and reduced computational cost offered by meshless approaches. The approach is strengthened by a strategic choice of shape parameter, which mitigates the well-known sensitivity issue inherent to RBFs, thereby enhancing the overall robustness and reliability of the numerical solution across varying spatial resolutions. Various test problems are examined, and the simulation results are compared with exact solutions and prior studies to demonstrate the superior performance and accuracy of the proposed approach.

Mathematics Subject Classification (2020): 65M06, 65M12

Key words and Phrases: PDEs; Discretization; Optimization; Hybrid block method; Mesh-based approaches; Meshless methods; RBF-FD; OMBM.

Email addresses: nazihah@uum.edu.my (Nazihah Ahmad); hizam@uum.edu.my (Kamarun Hizam Mansor); dybilel@yahoo.fr (Bilal Charmouti)*

Received December 11, 2025; Accepted January 5, 2026; Online February 4, 2026

1. Introduction

The resolution process of PDEs involves distinct phases. The first phase is the discretization of the continuous problem, which represents the problem spatially and temporally using discrete points or nodes. In case these discrete nodes are following a predefined arrangement with an established connectivity between them, the discretization method is called the mesh-based method, where the grid (mesh) is generated. This mesh can be regular or structured if the points appear in a uniform arrangement (regular pattern), and irregular if not the case as shown in Figure 1. On the other hand, if the scattered points are distributed without a fixed grid and predefined connectivity, the discretization is made by a meshless method, which is expanded in the next section. Discretization approximates derivatives at those discrete points using the methods like finite differences, which transform the PDE into a system of ODEs during semi-discretization. Subsequently, solution methods like Runge-Kutta [1] or block methods [2] are applied as ODE solvers, leading to a set of discrete algebraic equations. Full discretization directly yields this system, which is then solved to get the numerical solution. The next phase includes the analysis, interpretation, and visualization of results. To assess and validate the performance of the numerical method, a comparison of the numerical results is employed with known analytical solutions. Furthermore, an optimization task fine-tunes parameters or algorithms, enhancing the efficiency and convergence of this numerical method. Finally, the resolution process concludes with comparing the results with other methods, validating the method's performance. This structured flow ensures a systematic and comprehensive approach for solving PDEs numerically.

Therefore, discretization is a fundamental step in the process of approximating PDEs. It is the process of approximating a continuous mathematical model by dividing the problem into a finite set of discrete elements or points. This phase has a crucial impact on the effectiveness of the numerical method; it runs through the mesh-based method or meshless method. The first one relies on regular grid generation, a process that is often time-consuming and challenging, particularly for complex geometries, such as the FDM [4], FEM [5], FVM [6], boundary element method (BEM) [7], spectral method (SM) [8], and domain decomposition methods (DDM) [9]. In contrast, the meshless methods (MMs) eliminate the need for predefined grids or meshes, they use scattered or irregularly distributed points (nodes) to approximate the solution to PDEs. This feature provides more flexibility in handling complex geometry and leads to higher accuracy, with less consuming time [10] and less computational cost [11].

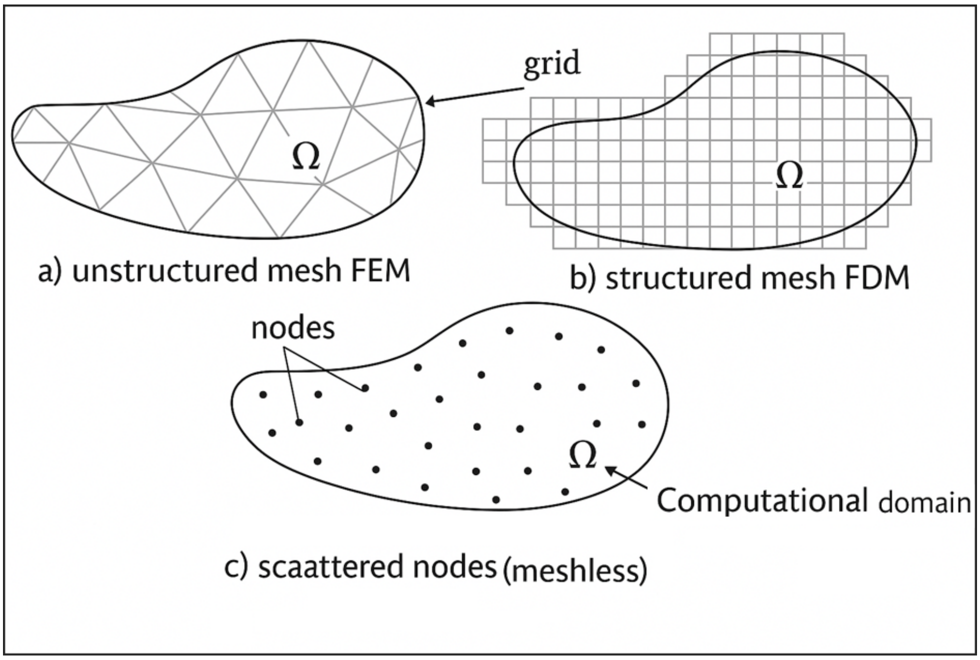

Figure 1: Examples of Meshless and Mesh-based Methods [3]

1.1 Meshless Methods

Partial differential equations (PDEs) arise in a wide range of scientific and engineering problems, and a variety of numerical methods have been developed to solve them. Among these, meshless methods—such as the moving least squares method [12], diffuse element method (DEM) [13], element-free Galerkin method (EFGM) [14], hp-clouds [15], partition of unity finite element method (PU-FEM) [16], reproducing kernel particle method (RKPM) [17], meshless local Petrov–Galerkin (MLPG) method [18], point collocation method (PCM) [19], and radial basis function (RBF) methods [20]—offer flexibility in handling complex geometries without the need for predefined meshes.

Meshless methods approximate the solution using scattered nodes rather than a structured mesh [22]. This allows greater adaptability to irregular domains and moving boundaries. For example, the smooth particle hydrodynamics (SPH) method [21] is known for its conservation properties and efficiency in large-scale and multiphase problems, though it suffers from stability and consistency issues. To address such limitations, refined methods have been introduced—e.g., the corrected SPH (or RKPM) [17] and EFG methods [14], which use moving least squares (MLS) interpolation to improve accuracy and stability.

Despite ongoing advancements, meshless methods still face several challenges. Many lack rigorous mathematical foundations, including established global error estimates and comprehensive stability analyses [23,24]. Practical difficulties also remain in areas such as modeling complex fracture patterns, high computational costs, and the efficient generation of node distributions. Furthermore, while strong form collocation offers computational advantages, it has received less attention compared to weak form (e.g., Galerkin) meshfree approaches, especially in fields like fracture mechanics and large deformation analysis [25].

One of the most promising meshless techniques is the radial basis function (RBF) method, which uses distance-based interpolation functions and is inherently mesh-independent [20]. Its simplicity in arbitrary spatial dimensions makes it attractive, although global RBF approaches suffer from computational inefficiencies as the number of nodes increases [26]. To mitigate this, localized RBF methods have been developed, including RBF-FD [28–30], Hermite-type radial point interpolation [31], local MQ differential quadrature (MQ-DQ) [32,33], subdomain RBF collocation [34], and integrated local/global RBF schemes [35,36]. Comprehensive reviews of these developments are found in [37,38].

The RBF-FD method, first proposed by Tolstykh [39] and later developed in [40], combines the accuracy of RBF interpolation with the computational efficiency of finite differences. It replaces globally supported RBFs with localized stencils, reducing the computational burden while preserving meshless flexibility. Despite its benefits, RBF-FD still faces open challenges, especially in coupling with time integration schemes and in handling large-scale problems [41].

1.2 Block Methods in Solving PDEs

Initially, block methods were firstly proposed by Milne [42] as self-starting multistep methods to get approximate solutions for a system of first order ODEs. They generate approximations simultaneously at multiple points, which saves computational time while preserving accuracy [43]. In these methods, data from several past points is required to get several solutions at future point. This powerful feature makes it a good alternative for solving ODEs, especially for stiff problems [44]. There are three different ways to derive the block methods, that are interpolation, Taylor series expansion, and numerical integration [43]. For the -th order IVP $y^{m} = f\left(x, y, y', \ldots, y^{(m-1)}\right)$, block methods with any desired order and step length can be derived using the procedure described in [45].

$$y_{n+\xi} = \sum_{i=0}^{m-1} \frac{(\xi h)^{i}}{i!} y_{n}^{(i)} + \sum_{i=0}^{k} \phi_{i}\, f_{n+i}, \qquad \xi = 1, 2, \ldots, k, \tag{1}$$

with derivatives

$$y_{n+\xi}^{(a)} = \sum_{i=0}^{m-(a+1)} \frac{(\xi h)^i}{i!} y_n^{(i+a)} + \sum_{i=0}^{k} w_{ia} \, f_{n+i}, \tag{2}$$

where: $a = 1_{(\xi=1,2,\ldots,k)}, 2_{(\xi=1,2,\ldots,k)}, \ldots, (m-1)_{(\xi=1,2,\ldots,k)}$,

ϕ_i and w_{ia} are constants, h is the step-size, k is the steplength and m is the order of the ODE.

There has been a limited amount of research in the literature addressing the solution of PDEs using block methods, the PDE is first discretized in space through the semi-discretization, which approximates the space derivatives using other mesh-based methods such as the finite difference method [46-48], B-spline approach [2], and compact difference method by [49]. This process results in a system of ODEs to be solved using the block method. These employed methods for spatial discretization are falling under the mesh-based category with its limitations, which open the door of using meshless methods rather than mesh-based methods in the discretization phase.

1.3 Combination of Block Methods and MMs

MMs have been introduced to eliminate the mesh-generating drawbacks such as discontinuities, computational cost and time [10,38,50]. However, as mentioned above it's important to note that the meshless methods still face some limitations including problems in stability compared to the mesh-based methods [24], and their accuracy can be sensitive to the choice of shape functions and basic functions. Therefore, by combining the accuracy and stability advantages of block methods with the capability of meshless methods to efficiently handle complex geometries at reduced computational cost and time, the overall quality of PDE solutions can be significantly improved. While block methods are valuable for ODEs, they are not often used and are not typically employed as standalone methods for solving PDEs [49]. They have been used with mesh-based methods, but with meshless methods the only work that has used this idea is presented in [51].

Meshless method (RBF-DQ) is combined with an optimized one-step hybrid block method, providing an efficient approach to achieve high accuracy while ensuring stability with less effort. Overall, the block method can be a powerful tool for solving PDEs numerically, but its effectiveness can highly depend on the chosen spatial discretization method, as it has a significant impact on the accuracy and stability of the solution [52,53].

The present work aims to extend the role of the block methods in solving PDEs by employing an optimized two-step hybrid block method with two intra-step points ($0 < r < 1 < s < 2$), coupled with meshless method RBF-FD with optimal shape parameter value, which helps to enhance stability and accuracy while reducing computational time and improving performance in handling complex geometries. Also, the proposed method extracts the optimal value of both step-size of the block method and shape parameter of the meshless method, to get an optimized method with better performance.

2. Methodology

This section describes the procedure of the proposed method, which mainly has been presented through two subsections. The first section discusses the meshless RBF-FD method that is employed to semi-discretize the PDE in spatial domain, which results in a system of ordinary differential equations (ODEs) with time as variable. The second section discusses how an optimized two-step hybrid block method with two off points is derived and then applied as a time-stepping algorithm to solve the former ODEs system. These two phases provide a system of algebraic equations can then be solved to give the final solution of the PDE.

2.1 Meshless RBF-FD Method

In the global RBF approach for numerically solving a PDE, interpolation is performed using all collocation points throughout the entire domain and boundary. As a result, the method often produces ill-conditioned matrices, leading to unstable and computationally demanding calculations, which makes these RBF collocation methods unsuitable for large-scale problems. To address these challenges, the RBF-FD method was developed as a local meshfree approach.

The discrete representation of a function $u(x)$ using the RBF interpolation function can be constructed from N scattered nodes and approximated by the following linear combination:

$$u(x_i) \simeq \tilde{u}(x_i) = \sum_{j=1}^{N} \alpha_j \phi\left(\left\|x_i - x_j\right\|\right), \tag{3}$$

where α_i are the interpolation coefficients, and $\phi\left(\left\|\mathbf{x}_i - \mathbf{x}_j\right\|\right)$ denotes radial basis functions such as the multiquadric (MQ), inverse multiquadric (IMQ), and Gaussian functions [54, 55]. Here, $\|\cdot\|$ represents the standard Euclidean norm. In the present study, the multiquadric (MQ) radial basis function (see Eq. (4)) is employed.

$$\phi\left(\left\|x_i - x_j\right\|\right) = \sqrt{\left\|x_i - x_j\right\|^2 + c^2}, \tag{4}$$

where $c > 0$ is the shape parameter to be selected.

Consider the PDE boundary value problem with Dirichlet boundary conditions

$$\begin{aligned} \mathcal{L}u &= f \text{ on } \Omega, \\ u &= g \text{ on } \partial\Omega. \end{aligned} \tag{5}$$

where $\mathcal{L}$ denotes the space differential operator, f and g are known functions.

For solving Eq. 5, the key step in RBF-FD calculations is to determine each node within a uniform set of N nodes $\{x_i\}_{i=1}^{N} \in \Omega$ in the spatial domain Ω, with a step size $h = x_{i+1} - x_i$. Each node x_i is associated with n ($n = 3$ in this paper) nearest neighbouring points $\{x_j\}_{j=1}^{n} \subseteq \{x_i\}_{i=1}^{N}$. For example, the subset $\{x_{i-1}, x_i, x_{i+1}\}$ with three elements is assigned to x_i.

The approximation RBF-FD formula for the derivative of the function $u(x,t)$ at the node x_i in Eq. (5) can be presented as follows[29, 56, 57]:

$$\mathcal{L}u(x_i,t) \simeq \sum_{j=i-1}^{i+1} w_j^{(m)} u(x_j,t), \tag{6}$$

where w_j are the weighted coefficients to be determined by solving the following linear system of n equations in m order of derivative:

$$\mathcal{L}\phi\left(\left\|x_i - x_j\right\|\right) \simeq \sum_{j=i-1}^{j=i+1} w_j^{(m)} \phi\left(\left\|x_i - x_j\right\|\right), \tag{7}$$

Eq. 7 can also be represented in form of matrices $Aw = B$, where the weighted coefficients matrix w can be found by solving $w = A^{-1}B$,

$$\begin{bmatrix} \phi\left(\left\|x_{i-1} - x_{i-1}\right\|\right) & \phi\left(\left\|x_i - x_{i-1}\right\|\right) & \phi\left(\left\|x_{i+1} - x_{i-1}\right\|\right) \\ \phi\left(\left\|x_{i-1} - x_i\right\|\right) & \phi\left(\left\|x_i - x_i\right\|\right) & \phi\left(\left\|x_{i+1} - x_i\right\|\right) \\ \phi\left(\left\|x_{i-1} - x_{i+1}\right\|\right) & \phi\left(\left\|x_i - x_{i+1}\right\|\right) & \phi\left(\left\|x_{i+1} - x_{i+1}\right\|\right) \end{bmatrix} \begin{bmatrix} w_{i-1}^{(m)} \\ w_i^{(m)} \\ w_{i+1}^{(m)} \end{bmatrix} = \begin{bmatrix} \mathcal{L}\phi\left(\left\|x_i - x_{i-1}\right\|\right) \\ \mathcal{L}\phi\left(\left\|x_i - x_i\right\|\right) \\ \mathcal{L}\phi\left(\left\|x_i - x_{i+1}\right\|\right) \end{bmatrix}, \tag{8}$$

$$\begin{bmatrix} \phi(0) & \phi(h) & \phi(2h) \\ \phi(h) & \phi(0) & \phi(h) \\ \phi(2h) & \phi(h) & \phi(0) \end{bmatrix} \begin{bmatrix} w_{i-1}^{(m)} \\ w_i^{(m)} \\ w_{i+1}^{(m)} \end{bmatrix} = \begin{bmatrix} \mathcal{L}\phi(h) \\ \mathcal{L}\phi(0) \\ \mathcal{L}\phi(-h) \end{bmatrix}, \tag{9}$$

For the first derivative $\mathcal{L} = \dfrac{d}{dx}$

$$\begin{bmatrix} \sqrt{c^2} & \sqrt{c^2+h^2} & \sqrt{c^2+4h^2} \\ \sqrt{c^2+h^2} & \sqrt{c^2} & \sqrt{c^2+h^2} \\ \sqrt{c^2+4h^2} & \sqrt{c^2+h^2} & \sqrt{c^2} \end{bmatrix} \begin{bmatrix} w_{i-1}^{(1)} \\ w_i^{(1)} \\ w_{i+1}^{(1)} \end{bmatrix} = \begin{bmatrix} \dfrac{h}{\sqrt{c^2+h^2}} \\ 0 \\ \dfrac{-h}{\sqrt{c^2+h^2}} \end{bmatrix}, \tag{10}$$

$$\begin{bmatrix} w_{i-1}^{(1)} \\ w_i^{(1)} \\ w_{i+1}^{(1)} \end{bmatrix} = \begin{bmatrix} \sqrt{c^2} & \sqrt{c^2+h^2} & \sqrt{c^2+4h^2} \\ \sqrt{c^2+h^2} & \sqrt{c^2} & \sqrt{c^2+h^2} \\ \sqrt{c^2+4h^2} & \sqrt{c^2+h^2} & \sqrt{c^2} \end{bmatrix}^{-1} \begin{bmatrix} \dfrac{h}{\sqrt{c^2+h^2}} \\ 0 \\ \dfrac{-h}{\sqrt{c^2+h^2}} \end{bmatrix}, \tag{11}$$

For the second derivative $\mathcal{L} = \dfrac{d^2}{dx^2}$

$$\begin{bmatrix} \sqrt{c^2} & \sqrt{c^2+h^2} & \sqrt{c^2+4h^2} \\ \sqrt{c^2+h^2} & \sqrt{c^2} & \sqrt{c^2+h^2} \\ \sqrt{c^2+4h^2} & \sqrt{c^2+h^2} & \sqrt{c^2} \end{bmatrix} \begin{bmatrix} w_{i-1}^{(2)} \\ w_i^{(2)} \\ w_{i+1}^{(2)} \end{bmatrix} = \begin{bmatrix} \dfrac{c^2}{\left(c^2+h^2\right)^{3/2}} \\ \dfrac{1}{c} \\ \dfrac{c^2}{\left(c^2+h^2\right)^{3/2}} \end{bmatrix}, \tag{12}$$

$$\begin{bmatrix} w_{i-1}^{(2)} \\ w_i^{(2)} \\ w_{i+1}^{(2)} \end{bmatrix} = \begin{bmatrix} \sqrt{c^2} & \sqrt{c^2+h^2} & \sqrt{c^2+4h^2} \\ \sqrt{c^2+h^2} & \sqrt{c^2} & \sqrt{c^2+h^2} \\ \sqrt{c^2+4h^2} & \sqrt{c^2+h^2} & \sqrt{c^2} \end{bmatrix}^{-1} \begin{bmatrix} \dfrac{c^2}{\left(c^2+h^2\right)^{3/2}} \\ \dfrac{1}{c} \\ \dfrac{c^2}{\left(c^2+h^2\right)^{3/2}} \end{bmatrix}. \tag{13}$$

This process yields a system of initial value problems (IVPs), which are then solved using a time-stepping scheme specifically, the optimized two-step hybrid block method employed in our study.

Regarding the order of the spatial discretization, a Taylor series expansion of the RBF-FD stencil about the node x_i yields the local truncation error for the first spatial derivative as

$$\mathcal{T}^{(1)}(x_i) = \frac{h^2}{6} u_i^{(3)} + \frac{h^2}{2c(h)^2} u_i' + O\left(h^4 + \frac{h^4}{c(h)^4} \right),$$

Similarly, for the second spatial derivative, the truncation error takes the form

$$\mathcal{T}^{(2)}(x_i) = C_1 h^2 u_i^{(4)} + C_2 \frac{h^2}{c(h)^2} u_i'' + O(h^4).$$

where C_1 and C_2 are constants independent of the grid spacing. In both cases, the leading error terms are proportional to h^2, confirming that the standard RBF-FD discretization based on the three-node stencil achieves second-order accuracy in space.

2.2. Optimal Shape Parameter

While RBFs demonstrate exceptional generalization capabilities, a significant challenge arises in handling partial differentiation. Selecting the appropriate shape parameters for the radial basis function is one of these critical challenges, as this parameter strongly influences the RBF approximation. Choosing suitable values greatly enhances the stability and accuracy of the computational results [57, 58]. As motioned in [59], there is a trade-off between interpolation error and matrix conditioning: reducing the error often results in poorly conditioned matrices, while improving matrix conditioning usually increases the error. Larger shape parameters improve matrix conditioning but reduce accuracy. [60] explored how the accuracy of solving convective PDEs is influenced by the RBF type, shape parameter, and time integration length.

Many efforts have been made to solve this problem. For instance, an early adaptive approach was introduced by Hardy [61], suggesting $\varepsilon = \frac{1}{0.815d}$, where d is the average distance to the nearest neighbour. $d = \frac{1}{N}\sum_{i=1}^{N} d_i$, N is the total number of interpolation nodes and d_i is the distance of node i to its nearest neighbour. After that, Franke [62] proposed an adaptive shape parameter, $\varepsilon = 0.8\frac{\sqrt{N}}{D}$, where D represents the diameter of the smallest circle that encompasses all the nodes. Wahba [63] presented a generalized cross-validation (GCV). Carlson and Foley used RMS error to determine ε [64]. Stein maximized the likelihood function in [65]. A genetic algorithm to determine ε for the solution of ODEs was proposed in [66]. Some articles focused on identifying an interval for the shape parameter, such as [67], which introduced an algorithm to find a variable shape parameter using a valid interval. [68] involves adding a loop over ε to find an interval rather than a single value, without minimizing or estimating an error function, where the suitable values of ε are identified by considering the actual convergence behaviour of the problem. A particle swarm optimization algorithm was proposed by Javad [69] to find a good shape parameter. Alternative methods focus on locally modifying the shape parameters. For instance, in [70], prediction functions are utilized to evaluate the interpolation error and determine the optimal shape parameter. In [71], a multilevel algorithm is introduced to find a near-optimal value. Another approach to tackle this issue is by exploring shape parameter expansions using advanced techniques, such as allowing complex values or applying efficient rational approximation methods [72, 73]. A new variable shape parameter method with neural networks was suggested in [60]. The study made in [30] focuses on selecting the optimal shape parameter value based on minimizing the approximation error when solving a PDE using the local RBF-FD method.

Following the technique introduced in [51], the proposed OMBM selects the RBF shape parameter $c > 0$ from a prescribed interval by minimizing the mismatch between the exact spatial derivative of the initial condition and its local RBF-FD approximation. Let

$$r(c) = \left(Du(x_i,0) - \mathcal{L}_c u(x_i,0)\right)_{i=2}^{N-1}, \tag{14}$$

$$c^* = \arg\min_{c\in[c_{\min},c_{\max}]} \left\| r(c) \right\|, \tag{15}$$

where D is the true spatial differentiation operator and $\mathcal{L}_c$ is the local RBF-FD operator parameterized by c. In practice, c^* is grid-dependent and varies with the number of nodes N via the spatial step $h = (x_{\max} - x_{\min})/(N-1)$; thus c^* should be re-estimated whenever N (and hence h) changes.

Algorithm 1 Pseudocode: Optimal Shape Parameter (OMBM)

```
Inputs: $u(\cdot,0), \{x_i\}, [c_{min}, c_{max}]$, $norm$, $tol$.
i) Grid setup .1
    $h \leftarrow (x_{max} - x_{min})/(N-1)$.
```

```
4: ii) Candidate search
5: linspace $\mathfrak{C} \leftarrow$ linspace $(c_{min}, c_{max}, M)$.
6: iii) Error evaluation
7: **For** each $c \in \mathfrak{C}$ do
8:     Compute $E(c)=\|Du(x_i,0) - L_c u(x_i,0)\|$ over interior nodes. \\
9: **End for**
10: iv) Selection and refinement
11: $c^* \leftarrow \arg\min\_\{c \in \mathfrak{C}\} E(c)$.
12: $[c_{min}, c_{max}] \leftarrow [c^*(1-\rho), c^*(1+\rho)]$, $\mathfrak{C} \leftarrow$ linspace $(c_{min}, c_{max}, M)$.
13: v) Stopping and output
14: **If** relative changes of $c^*$ and $E(c) < tol$.
15:     Return $c^*$ (grid-dependent via N through h).
16: **Else** go to step 6.
```

Optimal shape parameter selection reduces RBF sensitivity by balancing accuracy and stability. This ensures consistent performance across different spatial resolutions, making error less dependent on the number of nodes. The method maintains spectral convergence while providing reliable results for diverse computational applications.

2.3. Optimized two-step hybrid block Method for Time integration}

The two-step block method has proven to be an effective approach for solving initial-value problems, due to its notable features, including stability, and convergence [74]. The optimized two-step hybrid block method with two intra-step grid points ($0 < r < 1 < s < 2$) has been introduced in [75], which addressed the balance between accuracy and grid resolution, further enhanced the strengths of the block method, particularly its accuracy.

Thus, the optimized two-step hybrid block approach can be considered as a good choice to be a stepping time method to approximate the change of the function $u(x,t)$ in time. The time stepping is described by a first-order initial value problems (ODEs), of the form:

$$u'(t) = f(t,u), \qquad u(t_0) = u_0. \tag{16}$$

The solution to the problem in Eq. (16) is approximated using the following power series expansion:

$$u(t) \simeq \sum_{j=0}^{v+m-1} a_j t^j, \tag{17}$$

where, v indicates the number of interpolation points, which corresponds to the order of the differential equation, m denotes the number of collocation points, while a_j are real coefficients to be determined.

The first derivative of Eq. (17):

$$u'^{(t)} \simeq \sum_{j=1}^{v+m-1} j a_j t^{j-1}. \tag{18}$$

To derive this method, Eq. (17) is interpolated at t_n ($m = 1$), while Eq. (18) is collocated at the points , t_n, t_{n+r}, t_{n+1},t_{n+s}, and, t_{n+2} $(v = 5)$ as shown in Figure 2.

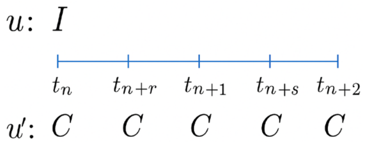

Figure 2: Interpolation and collocation strategy for two step hybrid block method with two off-step points for solving first order ODEs.

This produces a system of equations which can be written in a matrix form as below:

$$\begin{bmatrix} 1 & t_n & t_n^2 & t_n^3 & t_n^4 & t_n^5 \\ 0 & 1 & 2t_n & 3t_n^2 & 4t_n^3 & 5t_n^4 \\ 0 & 1 & 2t_{n+r} & 3t_{n+r}^2 & 4t_{n+r}^3 & 5t_{n+r}^4 \\ 0 & 1 & 2t_{n+1} & 3t_{n+1}^2 & 4t_{n+1}^3 & 5t_{n+1}^4 \\ 0 & 1 & 2t_{n+s} & 3t_{n+s}^2 & 4t_{n+s}^3 & 5t_{n+s}^4 \\ 0 & 1 & 2t_{n+2} & 3t_{n+2}^2 & 4t_{n+2}^3 & 5t_{n+2}^4 \end{bmatrix} \begin{bmatrix} a_0 \\ a_1 \\ a_2 \\ a_3 \\ a_4 \\ a_5 \end{bmatrix} = \begin{bmatrix} u_n \\ f_n \\ f_{n+r} \\ f_{n+1} \\ f_{n+s} \\ f_{n+2} \end{bmatrix}, \tag{19}$$

The Gaussian elimination method is applied on Eq. (19) to find the coefficients a_0, a_1, a_2, a_3, a_4, and a_5, which are then substituted into Eq. (17) to give an implicit scheme of the form:

$$u(t) \simeq \alpha_0 u_n + k\left(\beta_0 f_n + \beta_r f_{n+r} + \beta_1 f_{n+1} + \beta_s f_{n+s} + \beta_2 f_{n+2}\right) \tag{20}$$

where k represents the time-step

$$\begin{aligned} \alpha_0 &= 1 \\ \beta_0 &= \frac{t\left(5r\left(2s(2t^2 - 9t + 12) - 3(t-2)^2 t\right) + t\left(t(12t^2 - 45t + 40) - 15s(t-2)^2\right)\right)}{120rs} \\ \beta_r &= \frac{t^2\left(t(12t^2 - 45t + 40) - 15s(t-2)^2\right)}{60(r-2)(r-1)r(r-s)} \\ \beta_1 &= \frac{t^2\left(5r\left(4s(t-3) + (8-3t)t\right) + t\left(6t(2t-5) - 5s(3t-8)\right)\right)}{60(r-1)(s-1)} \\ \beta_s &= \frac{t^2\left(15r(t-2)^2 + t(-12t^2 + 45t - 40)\right)}{60s(s^2 - 3s + 2)(r-s)} \\ \beta_2 &= \frac{t^2\left(5r\left(s(4t-6) + (4-3t)t\right) + t\left(3t(4t-5) - 5s(3t-4)\right)\right)}{120(r-2)(s-2)} \end{aligned}$$

Evaluating Eq. (20) at the non-interpolating point t_{n+r}, t_{n+1}, t_{n+s}, and t_{n+2} yields the hybrid block method represented by the following set of four equations:

$$\begin{aligned} u_{n+r} = u_n &+ \frac{kr\left(-3r^3 + 60s + 5r^2(1+3s) - 10r(2+3s)\right) f_n}{120s} \\ &+ \frac{kr\left(12r^3 - 60s - 15r^2(3+s) + 20r(2+3s)\right) f_{n+r}}{60(2 - 3r + r^2)(r-s)} \\ &+ \frac{kr^3\left(3r^2 + 20s - 5r(2+s)\right) f_{n+1}}{60(-1+r)(-1+s)} + \frac{kr^3\left(20 - 15r + 3r^2\right) f_{n+s}}{60(r-s)s(2 - 3s + s^2)} \\ &+ \frac{kr^3\left(-3r^2 - 10s + 5r(1+s)\right) f_{n+2}}{120(-2+r)(-2+s)}. \end{aligned} \tag{21}$$

$$\begin{aligned} u_{n+1} = u_n &+ \frac{k\left(7 - 15s + 5r(-3 + 10s)\right) f_n}{120rs} + \frac{k\left(7 - 15s\right) f_{n+r}}{60r(2 - 3r + r^2)(r-s)} \\ &+ \frac{k\left(18 - 25s + 5r(-5 + 8s)\right) f_{n+1}}{60(-1+r)(-1+s)} + \frac{k\left(-7 + 15r\right) f_{n+s}}{60(r-s)s(2 - 3s + s^2)} \\ &+ \frac{k\left(-3 + r(5 - 10s) + 5s\right) f_{n+2}}{120(-2+r)(-2+s)}. \end{aligned} \tag{22}$$

$$
\begin{aligned}
u_{n+s} = u_n &+ \frac{ks\big(s(-20+15s-3s^2)+5r(12-6s+s^2)\big)f_n}{120r} - \frac{ks^3\big(20-15s+3s^2\big)f_{n+r}}{60r(2-3r+r^2)(r-s)} \\
&+ \frac{ks^3\big(-5r(-4+s)+s(-10+3s)\big)f_{n+1}}{60(-1+r)(-1+s)} \\
&+ \frac{ks\big(15r(-2+s)^2+s(-40+45s-12s^2)\big)f_{n+s}}{60(r-s)(2-3s+s^2)} \\
&+ \frac{ks^3\big(5r(-2+s)+(5-3s)s\big)f_{n+2}}{120(-2+r)(-2+s)}.
\end{aligned}
\tag{23}
$$

$$
\begin{aligned}
u_{n+2} = u_n &+ \frac{k(-2+5rs)f_n}{15rs} - \frac{4kf_{n+r}}{15r(2-3r+r^2)(r-s)} + \frac{4k\big(6+5r(-1+s)-5s\big)f_{n+1}}{15(-1+r)(-1+s)} \\
&+ \frac{4kf_{n+s}}{15(r-s)s(2-3s+s^2)} + \frac{k\big(18+5r(-2+s)-10s\big)f_{n+2}}{15(-2+r)(-2+s)}.
\end{aligned}
\tag{24}
$$

where k denotes the fixed step-size in time, r and s are determined by optimizing the local truncation errors for u_{n+1} and u_{n+2} in Eq. (22) and Eq. (24) respectively. This leads to the following expressions:

$$
\begin{aligned}
&r = \frac{1}{3}\left(3-\sqrt{3}\right) \approx 0.42265, \\
&s = 2-r \approx 1.57735, \qquad (0 < r < 1 < s < 2).
\end{aligned}
\tag{25}
$$

Substituting the chosen intra-step points r and s, and replacing $f_{n+r}, f_{n+1}, f_{n+s}, f_{n+2}$ in Eqs. (21–24) with their RBF-FD spatial approximations from Eq. (6), yields the following fully discrete scheme of the proposed method, ready for implementation. The resulting nonlinear algebraic system is then solved in MATLAB.

Within one 4-step block let

$$\mathcal{T}_1 = r, \qquad \mathcal{T}_2 = 1, \qquad \mathcal{T}_3 = s, \qquad \mathcal{T}_4 = 2$$

Index the five-time levels by

$$\ell = 0 \leftrightarrow n, \qquad \ell = 1 \leftrightarrow n+r, \qquad \ell = 2 \leftrightarrow n+1, \qquad \ell = 3 \leftrightarrow n+s, \qquad \ell = 4 \leftrightarrow n+2$$

With time step k, the four equations at each interior node can be written for m = 1, ..., 4 as
The coefficients $a_{m,l}$ are defined as follows:

$$\left(I - \frac{k}{120}a_{m,m}\mathcal{L}\right)u^{n+\tau_m} + \sum_{\ell \neq m}\left(-\frac{k}{120}a_{m,\ell}\mathcal{L}\right)u^{n+\ell} = u^n + \frac{k}{120}a_{m,0}\mathcal{L}u^n, \tag{26}$$

- Row m = 1 (equation at n + n)

$$a_{1,0} = \frac{2}{9(\sqrt{3}+3)}\left(3-\sqrt{3}\right)\left(168+85\sqrt{3}\right),$$

$$a_{1,1} = \frac{2}{9\left(\sqrt{3}+3\right)}\left(3-\sqrt{3}\right)\left(351+180\sqrt{3}\right),$$

$$a_{1,2} = \frac{2}{9\left(\sqrt{3}+3\right)}\left(\sqrt{3}-3\right)\left(3+5\sqrt{3}\right),$$

$$a_{1,3} = \frac{18}{\sqrt{3}+3}\left(3-\sqrt{3}\right),$$

$$a_{1,4} = \frac{2}{9\left(\sqrt{3}+3\right)}\left(12+5\sqrt{3}\right)\left(\sqrt{3}-3\right).$$

- Row $m = 2$ (equation at $n + 1$)

$$a_{2,0} = \frac{31}{2}, \qquad a_{2,1} = \frac{72+45\sqrt{3}}{2}, \qquad a_{2,2} = 32, \qquad a_{2,3} = \frac{72-45\sqrt{3}}{2}, \quad a_{2,4} = \frac{1}{2}.$$

- Row $m = 3$ (equation at $n + s$)

$$a_{3,0} = \frac{2}{9\left(\sqrt{3}-3\right)}\left(3+\sqrt{3}\right)\left(85\sqrt{3}-168\right),$$

$$a_{3,1} = -\frac{18}{\sqrt{3}-3}\left(3+\sqrt{3}\right),$$

$$a_{3,2} = \frac{2}{9\left(\sqrt{3}-3\right)}\left(48-80\sqrt{3}\right)\left(3+\sqrt{3}\right),$$

$$a_{3,3} = \frac{2}{9\left(\sqrt{3}-3\right)}\left(3+\sqrt{3}\right)\left(180\sqrt{3}-351\right),$$

$$a_{3,4} = \frac{2}{9\left(\sqrt{3}+3\right)}\left(12-5\sqrt{3}\right)\left(3+\sqrt{3}\right).$$

- Row $m = 4$ (equation at $n + 2$)

$$a_{4,0} = 16, \qquad a_{4,1} = 72, \qquad a_{4,2} = 64, \qquad a_{4,3} = 72, \qquad a_{4,4} = 16.$$

The optimized two-step hybrid block method with two off-step points can be written in the compact form

$$A_1 U_n = A_0 U_{n-1} + k\left[B_1 F_n + B_0 F_{n-1}\right],$$

where $A_1 = I_4$, A_0 is a matrix with ones in the first column, and B_0 and B_1 are coefficient matrices containing rational and irrational terms.

To determine the order of the method, the associated linear difference operator is constructed and expanded in a Taylor series about $t = t_n$, yielding

$$L\left[u(t,k)\right] = C_0 u(t) + C_1 k u'(t) + C_2 k^2 u''(t) + \cdots.$$

The method is said to be of order p if $C_0 = C_1 = \cdots = C_p = 0$ and $C_{p+1} \neq 0$. For the present method, the computed error constants satisfy

$$C_0 = C_1 = C_2 = C_3 = C_4 = C_5 = 0, \quad C_6 = \begin{bmatrix} \frac{1}{4860} \\ \frac{1}{4860} \\ 0 \\ 0 \end{bmatrix} \neq 0.$$

Consequently,

$$L\left[u(t,k)\right] = C_6 k^6 u^{(6)}(t) + \mathcal{O}(k^7),$$

which confirms that the optimized two-step hybrid block method is of order $p = 5$ and satisfies the consistency condition for linear multistep methods.

Combining the spatial and temporal discretization, the overall accuracy of the fully discrete scheme can be established. The RBF-FD approximation employed for the spatial derivatives is second-order accurate, yielding a local spatial truncation error of order $\mathcal{O}(h^2)$, while the two-step hybrid block method used for time integration possesses a fifth-order local truncation error of order $\mathcal{O}(k^5)$.

Although the numerical experiments in this work focus on one-dimensional problems, the proposed method naturally extends to higher-dimensional PDEs. The time discretization based on the two-step hybrid block method is independent of the spatial dimension, while the spatial discretization can be directly generalized using the RBF-FD framework by employing multi-dimensional local stencils in $\mathbb{R}^2$ or $\mathbb{R}^3$. Therefore, the proposed approach remains applicable to higher-dimensional problems without modification of the time-integration strategy.

3. Numerical Results and Discussion

The effectiveness of the proposed method is evaluated through four numerical examples, demonstrating its efficiency and accuracy across different problem types. The first two examples focus on solving the one-dimensional heat equation under various initial and boundary conditions, highlighting the method's performance in handling parabolic partial differential equations. The last two examples address the coupled Burgers' equations, a nonlinear system commonly encountered in fluid dynamics and other applications, showcasing the method's ability to handle complex, multi-variable problems.

The evaluation is conducted by comparing the numerical results with the exact solutions, using the L_2 and L_∞ error norms. These error metrics provide a comprehensive measure of the method's accuracy, with L_2 capturing the overall deviation and L_∞ emphasizing the maximum error at any given point. The formulas for these error norms are as follows:

$$\begin{aligned} L_2 &= \left\| u_i^{\text{exact}} - u_i^{\text{num}} \right\|_2 = \sqrt{h \sum_{i=0}^{N} \left| u_i^{\text{exact}} - u_i^{\text{num}} \right|^2}, \\ L_\infty &= \left\| u_i^{\text{exact}} - u_i^{\text{num}} \right\|_\infty = \max_i \left| u_i^{\text{exact}} - u_i^{\text{num}} \right|, \end{aligned} \tag{27}$$

where u_i^{exact} and u_i^{num} denote the exact and approximate solutions evaluated at (x_i, t).

Test problem 1: Consider the nonlinear viscous Burgers' equation [76]:
Use a different font package

$$u_t = \epsilon u_{xx} - u u_x, \qquad t \geq 0 \tag{28}$$

Initial conditions:

$$u(x,0) = 2\epsilon\pi \frac{\frac{\sin(\pi x)}{4} + \sin(2\pi x)}{1 + \frac{\cos(\pi x)}{4} + \frac{\cos(2\pi x)}{4}} \tag{29}$$

Boundary conditions:

$$u(0, t) = u(2, t) = 0, \tag{30}$$

The exact solution is:

$$u(x,t) = 2\epsilon\pi \frac{\frac{\sin(\pi x)}{4} e^{-\pi^2 \epsilon^2 t} + \sin(2\pi x) e^{-4\pi^2 \epsilon^2 t}}{1 + \frac{\cos(\pi x)}{4} e^{-\pi^2 \epsilon^2 t} + \frac{\cos(2\pi x)}{4} e^{-4\pi^2 \epsilon^2 t}}, \tag{31}$$

We conduct experiments with 80 grid points and varied values of parameters ε. Solutions at $t = 0.1$ and $t = 1$ are benchmarked against the methods in [76] and [77]; Table 1 reports the L_∞ error. Figure 3 provides a two-dimensional view of the solution's evolution over time. Across all ϵ values, the proposed method achieves lower errors while using fewer time steps as in [76], showing a modest advantage for $\epsilon = 10^{-2}$, $\epsilon = 10^{-3}$, $\epsilon = 10^{-4}$, and $\epsilon = 10^{-5}$ a markedly larger one for $\epsilon = 10^{-6}$.

Table 1: L_∞ Error comparison for u in Problem 1 taking different values of ϵ.

ϵ	Mittal and Rohila [77]		Mehta et al., [76]		Present method (OMBM)	
	$t = 0.1$	$t = 1$	$t = 0.1$	$t = 1$	$t = 0.1$	$t = 1$
10^{-2}	4.67×10^{-3}	3.08×10^{-2}	4.26×10^{-3}	3.08×10^{-2}	1.45×10^{-3}	6.82×10^{-3}
10^{-3}	4.90×10^{-5}	3.95×10^{-4}	4.46×10^{-5}	4.30×10^{-4}	2.68×10^{-5}	2.24×10^{-4}
10^{-4}	4.92×10^{-7}	4.46×10^{-6}	4.48×10^{-7}	4.46×10^{-6}	2.85×10^{-7}	2.54×10^{-6}
10^{-5}	4.93×10^{-9}	4.48×10^{-8}	4.48×10^{-9}	4.48×10^{-8}	8.36×10^{-10}	7.52×10^{-9}
10^{-6}	4.53×10^{-11}	4.48×10^{-10}	4.48×10^{-11}	4.48×10^{-10}	4.46×10^{-15}	4.01×10^{-14}
Nt	100	100	2	2	2	2

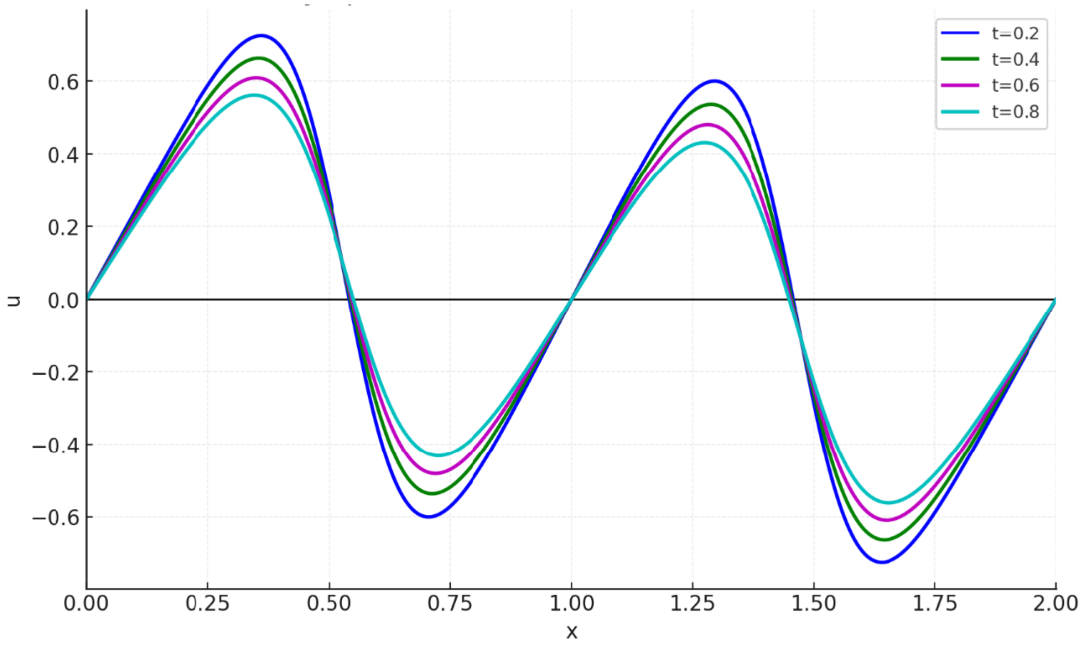

Figure 3: 2D visualization of numerical solution for u of problem 1 at $\epsilon = 10^{-2}$ with different values of t.

Test problem 2: Consider the coupled Burgers equation [78]:

$$\begin{aligned} &u_t - u_{xx} - 2uu_x + (uv)_x = 0, \\ &v_t - v_{xx} - 2vv_x + (uv)_x = 0, \end{aligned} \tag{32}$$

Initial conditions:

$$u(x,0) = v(x,0) = \sin(x), \qquad -\pi \le x \le \pi \tag{33}$$

Boundary conditions:

$$\begin{aligned} &u(-\pi,t) = u(\pi,t) = 0, \quad 0 \le t \le T \\ &v(-\pi,t) = v(\pi,t) = 0, \quad 0 \le t \le T \end{aligned} \tag{34}$$

The exact solution is:

$$u(x,t) = v(x,t) = e^{-t}\sin(x), \qquad -\pi \le x \le \pi, \quad 0 \le t \le T \tag{35}$$

Problem 2 addresses solving the coupled Burgers' equations with specified initial and boundary conditions using the proposed method. Figure 4 and Figure 5 illustrate both 3-D and 2-D visualizations of the exact and numerical solutions for u. Table 2 compares OMBM with the method from [51] at $t = 0.1$ for $k = 0.1$, varying values of N and c. Table 3 presents a comparison between OMBM and the methods in [79] at $t = 0.5$, considering $k = 0.1$, $N = 30$ (less grid points) for OMBM method and $N = 130$ for the methods in [79].

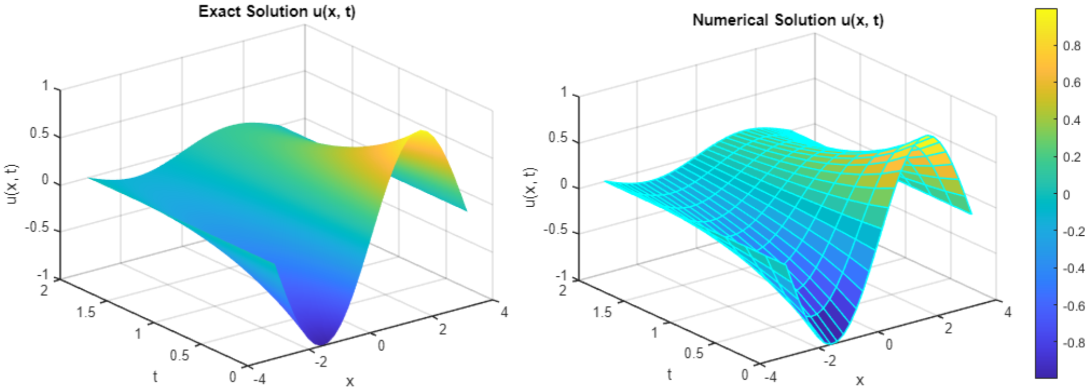

Figure 4: 3D visualization of exact (analytical) and numerical solution for u of problem 2 with $k = 0.1$, $t = 1$

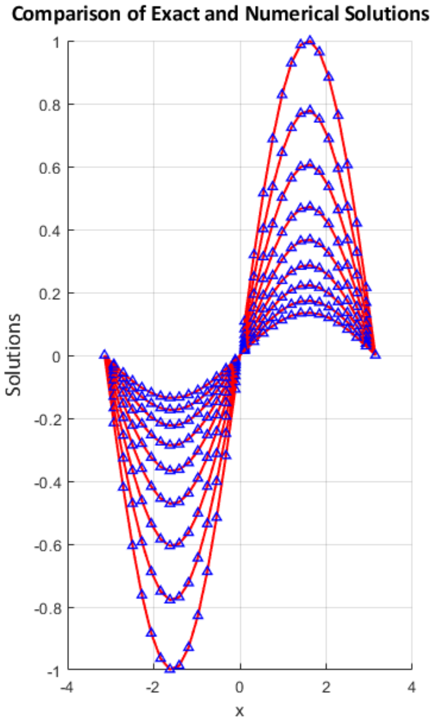

Figure 5: 2D visualization of exact (analytical) and numerical solution for u of problem 2 with $k = 0.1$, $t = 1$

Table 2: Error comparison for u in Problem 2 at $t = 0.1$ for k =0.1 and different values of N

N	Kaur et al., [51]		c	Present method (OMBM)	
	L_∞	L_2		L_∞	L_2
10	1.8209×10^{-4}	3.3934×10^{-4}	3.4014	8.92808×10^{-12}	1.60687×10^{-11}
20	7.9202×10^{-6}	1.4031×10^{-5}	3.5285	9.22606×10^{-12}	1.54086×10^{-11}
30	9.2190×10^{-10}	1.0031×10^{-9}	3.5493	8.31268×10^{-12}	1.47554×10^{-11}

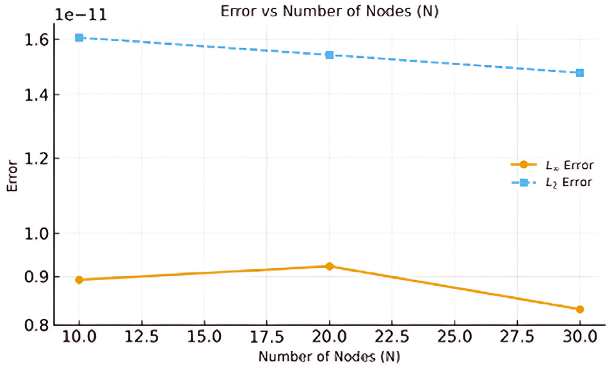

Figure 6: 2D visualization of errors vs number of nodes (N) of problem 2

Table 3: Error L_∞ comparison for u in Problem 2 at t = 0.5 for k =0.1

Method	N	L_∞
OMBM	30	2.79×10^{-11}
CBSLM3 [79]	130	4.27×10^{-7}
SC-SL$_1$ [79]	130	1.04×10^{-5}
SC-SL$_2$ [79]	130	4.03×10^{-7}
SC-SL$_3$ [79]	130	3.91×10^{-7}

Test problem 3: Consider the following coupled Burgers' equation of the form:

$$\begin{aligned} &u_t - \epsilon u_{xx} + 2uu_x - (uv)_x = 0, \\ &v_t - \epsilon v_{xx} + 2vv_x - (uv)_x = 0, \end{aligned} \tag{36}$$

Initial conditions:

$$u(x,0) = v(x,0) = \cos(\pi x), \qquad 0 \le x \le 1 \tag{37}$$

Boundary conditions:

$$u(0,t) = u(0,t) = e^{-\epsilon\pi^2 t}, \qquad 0 \le t \le Tv(1,t) = v(1,t) = -e^{-\epsilon\pi^2 t}, \qquad 0 \le t \le T \tag{38}$$

The exact solution is:

$$u(x,t) = v(x,t) = e^{-\epsilon\pi^2 t}\cos(\pi x), \qquad 0 \le x \le 1, 0 \le t \le T \tag{39}$$

where ϵ is positive kinematic viscous parameter depending on Reynolds number $\epsilon = 1/Re$, in this test case $\epsilon = 10^{-6}$.

In this problem, the results for u and u, presented in Table 4 and Table 5 respectively, are compared with the findings in [51, 80], considering N = 4, k = 0.1, c = 1.0159 and various values of t. Figure 7 and Figure 8 provide both 3D and 2D visualizations of the exact and numerical solutions for u, showcasing the accuracy of the proposed approach.

- Performance and convergence.

  The proposed OMBM scheme consistently outperforms existing approaches in our tests. Across all benchmarks, it delivers lower error norms for comparable costs and admits near-optimal parameter choices (node layout and shape parameter).

- Mesh independence.

  Beyond a modest node count, further refinement produces no appreciable change in the numerical solution Figure 6, indicating that the spatial discretization error is negligible relative to other sources. This mesh-independent behaviour confirms that our nodal distribution and shape parameter capture the solution effectively without unnecessary computational overhead.

- Robustness and efficiency.

  The solution remains stable under mesh refinement, attesting to the robustness of the method. Using the minimum number of nodes required to reach the mesh-independent regime ensures good accuracy at reasonable cost, avoiding superfluous refinement.

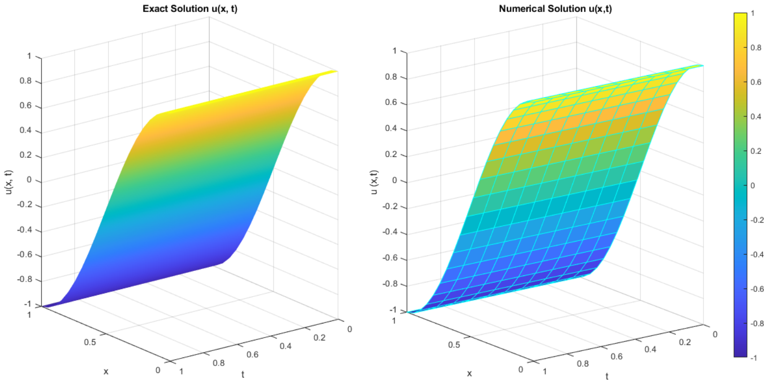

Figure 7: 3D visualization of exact (analytical) and numerical solution for u of problem 3 with $k = 0.1$, $T = 1$

Table 4: Error comparison for u in Problem 3 with N =4, k =0.1 and $\epsilon = 10^{-6}$

t	Shallal et al., [80]		Kaur et al., [51]		Present method (OMBM)	
	L_∞	L_2	L_∞	L_2	L_∞	L_2
0.1	1.8147×10^{-7}	1.2832×10^{-5}	5.0152×10^{-9}	3.1295×10^{-9}	4.8738×10^{-14}	3.9659×10^{-14}
0.3	5.4442×10^{-7}	3.8497×10^{-5}	1.4997×10^{-8}	9.3087×10^{-9}	4.8738×10^{-14}	3.9659×10^{-14}
0.5	9.0737×10^{-7}	6.4161×10^{-7}	2.9106×10^{-8}	1.5920×10^{-8}	4.8794×10^{-14}	3.9704×10^{-14}
0.7	1.2703×10^{-6}	8.9825×10^{-7}	5.3033×10^{-8}	2.7938×10^{-8}	4.8738×10^{-14}	3.9659×10^{-14}

Table 5: Error comparison for u in Problem 3 with $N = 4$, k =0.1 and $\epsilon = 10^{-6}$

t	Shallal et al., [80]		Kaur et al., [51]		Present method (OMBM)	
	L_∞	L_2	L_∞	L_2	L_∞	L_2
0.1	1.8147×10^{-7}	1.2832×10^{-5}	5.0152×10^{-9}	2.5350×10^{-9}	4.8738×10^{-14}	3.9659×10^{-14}
0.3	5.4442×10^{-7}	3.8497×10^{-5}	1.9921×10^{-8}	1.3377×10^{-8}	4.8738×10^{-14}	3.9659×10^{-14}
0.5	9.0737×10^{-7}	6.4161×10^{-7}	2.7001×10^{-8}	1.6748×10^{-8}	4.8794×10^{-14}	3.9704×10^{-14}
0.7	1.2703×10^{-6}	8.9825×10^{-7}	4.9534×10^{-8}	2.7948×10^{-8}	4.8738×10^{-14}	3.9659×10^{-14}

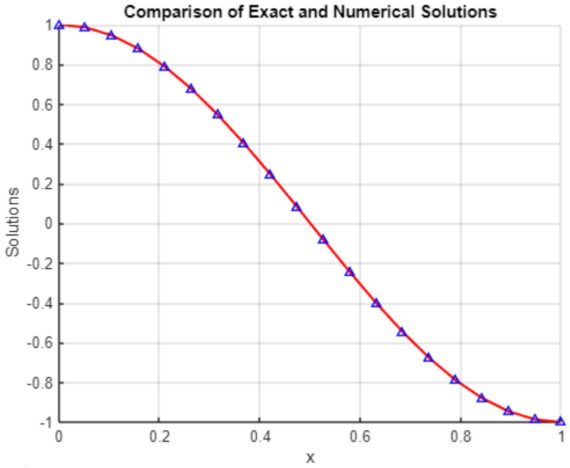

Figure 8: 2D visualization of exact (analytical) and numerical solution for u of problem 3 with $k = 0.1$, $T = 1$

4. Conclusion

This study introduced an Optimized Meshless Block Method (OMBM) for solving time-dependent partial differential equations by combining the RBF-FD technique for spatial discretization with a two-step hybrid block method for time integration. While this combination is capable of addressing several challenges associated with traditional numerical methods such as handling complex geometries and reducing computational cost, the present work has focused specifically on evaluating and demonstrating improvements in accuracy and robustness. Numerical experiments confirmed that the proposed OMBM method achieves high accuracy, verified convergence, and efficient use of computational resources.

For future work, various strategies can be explored to determine the optimal value of the shape parameter. Additionally, different types of RBFs can be employed, such as Gaussian and inverse multiquadric (IMQ), to assess their impact on the performance and accuracy of the method. These approaches could provide deeper insights and potentially improve the robustness and versatility of the solution method.

References

[1] Romeo, Giovanni. Elements of numerical mathematical economics with Excel: static and dynamic optimization. Academic Press, 2019. https://doi.org/10.1016/B978-0-12-817648-1.02003-X

[2] Ramos, H., Kaur, A., & Kanwar, V. (2022). Using a cubic B-spline method in conjunction with a one-step optimized hybrid block approach to solve nonlinear partial differential equations. Computational and Applied Mathematics, 41(1). https://doi.org/10.1007/s40314-021-01729-7

[3] Ferreira, L. A., & Mesquita, R. C. (2015). Graphical Interface for Electromagnetic Problem Solving Using Meshless Methods. In Article in Journal of Microwaves Optoelectronics and Electromagnetic Applications (Vol. 14, Issue 1).

[4] Courant, R., Friedrichs, K., & Lewy, H. (1928). Über die partiellen Differenzengleichungen der mathematischen Physik. Mathematische annalen, 100(1), 32-74. https://doi.org/10.1007/BF01448839

[5] Ciarlet, P. G., & Raviart, P. A. (1973). Maximum principle and uniform convergence for the finite element method. Computer methods in applied mechanics and engineering, 2(1), 17-31. https://doi.org/10.1016/0045-7825(73)90019-4

[6] Tian, M. , & C. Z. (1991). Quadratic element generalized differential methods for elliptic equations. Numer. Math. J. Chinese Univ, 13, 99-13.

[7] Costabel, M. (1987). Principles of boundary element methods. Computer Physics Reports, 6(1-6), 243-274. https://doi.org/10.1016/0167-7977(87)90014-1

[8] Bernardi, C., & Maday, Y. (1997). Spectral methods. Handbook of numerical analysis, 5, 209-485. https://doi.org/10.1016/S1570-8659(97)80003-8

[9] Smith, B. F. (1997). Domain Decomposition Methods for Partial Differential Equations (pp. 225-243). https://doi.org/10.1007/978-94-011-5412-3_8

[10] Fasshauer, G. E. (2007). Meshfree approximation methods with MATLAB (Vol. 6). World Scientific. https://doi.org/10.1142/6437

[11] Burkhardt, J., Wu, Y., Computing, Y. Z.-S. J. on S., & 2021, undefined. (2021). A unified meshfree pseudospectral method for solving both classical and fractional PDEs. SIAMJ Burkardt, Y Wu, Y ZhangSIAM Journal on Scientific Computing, 2021. https://doi.org/10.1137/20M1335959

[12] Eason, E. D. (1976). A review of least-squares methods for solving partial differential equations. International Journal for Numerical Methods in Engineering, 10(5), 1021-1046. https://doi.org/10.1002/nme.1620100505

[13] Nayroles, B., Touzot, G., & Villon, P. (1992). Generalizing the finite element method: Diffuse approximation and diffuse elements. Computational Mechanics, 10(5), https://doi.org/10.1007/BF00364252

[14] Belytschko, T., Lu, Y. Y., & Gu, L. (1994). Element-free Galerkin methods. International journal for numerical methods in engineering, 37(2), 229-256. https://doi.org/10.1002/nme.1620370205

[15] Duarte, C. A., & Oden, J. T. (1996). An hp adaptive method using clouds. Computer methods in applied mechanics and engineering, 139(1-4), 237-262. https://doi.org/10.1016/S0045-7825(96)01085-7

[16] Melenk, J. M., & Babuška, I. (1996). The partition of unity finite element method: basic theory and applications. Computer methods in applied mechanics and engineering, 139(1-4), 289-314. https://doi.org/10.1016/S0045-7825(96)01087-0

[17] Liu, Jun, S., & Zhang, Y. F. (1995). Reproducing kernel particle methods. International Journal for Numerical Methods in Fluids, 20(8-9), 1081-1106. https://doi.org/10.1002/fld.1650200824

[18] Atluri, S. N., & Zhu, T. (1998). A new meshless local Petrov-Galerkin (MLPG) approach in computational mechanics. Computational mechanics, 22(2), 117-127. https://doi.org/10.1007/s004660050346

[19] Aluru, N. (2000). A point collocation method based on reproducing kernel approximations. International Journal for Numerical Methods in Engineering, 47(6), 1083-1121. https://doi.org/10.1002/(SICI)1097-0207(20000228)47:6<1083::AID-NME816>3.0.CO;2-N

[20] Kansa, E. J. (1990). Multiquadrics-a scattered data approximation scheme with applications to computational fluid-dynamics-II. In Computers Math. Applic (Vol. 19, Issue 9). https://doi.org/10.1016/0898-1221(90)90271-K

[21] Monaghan, J. J. (2003). Smoothed Particle Hydrodynamics.

[22] Ahmad, I., Siraj-ul-Islam, & Khaliq, A. Q. M. (2017). Local RBF method for multi-dimensional partial differential equations. Computers & Mathematics with Applications, 74(2), 292-324. https://doi.org/10.1016/j.camwa.2017.04.026

[23] Slak, J. (2020). Adaptive RBF-FD method: PhD thesis (Doctoral dissertation, Univerza v Ljubljani, Fakulteta za matematiko in fiziko).

[24] Tillenius, M., Larsson, E., Lehto, E., & Flyer, N. (2015). A scalable RBF-FD method for atmospheric flow. Journal of Computational Physics, 298, 406-422. https://doi.org/10.1016/j.jcp.2015.06.003

[25] Chen, J.-S., Hillman, M., & Chi, S.-W. (2017). Meshfree Methods: Progress Made after 20 Years. Journal of Engineering Mechanics, 143(4), 04017001. https://doi.org/10.1061/(ASCE)EM.1943-7889.0001176

[26] Koushki, M., Jabbari, E., & Ahmadinia, M. (2020). Evaluating RBF methods for solving PDEs using Padua points distribution. Alexandria Engineering Journal, 59(5), 2999-3018. https://doi.org/10.1016/j.aej.2020.04.047

[27] Chen, W., Fu, Z. J., & Chen, C. S. (2014). Recent advances in radial basis function collocation methods (Vol. 768). Berlin: Springer https://doi.org/10.1007/978-3-642-39572-7

[28] G.B. Wright, B. Fornberg, Scattered node compact finite difference-type formulas generated from radial basis functions. J. Comput. Phys. 212(1), 99-123 (2006) https://doi.org/10.1016/j.jcp.2005.05.030

[29] V. Bayona, M. Moscoso, M. Carretero, M. Kindelan, RBF-FD formulas and convergence properties. J. Comput. Phys. 229(22), 8281-8295 (2010) https://doi.org/10.1016/j.jcp.2010.07.008

[30] V. Bayona, M. Moscoso, M. Kindelan, Optimal constant shape parameter for multiquadric based RBF-FD method. J. Comput. Phys. 230(19), 7384-7399 (2011) https://doi.org/10.1016/j.jcp.2011.06.005

[31] Y. Liu, Y.C. Hon, K.M. Liew, A meshfree Hermite-type radial point interpolation method for Kirchhoff plate problems. Int. J. Numer. Meth. Eng. 66(7), 1153-1178 (2006) https://doi.org/10.1002/nme.1587

[32] C. Shu, H. Ding, K.S. Yeo, Local radial basis function-based differential quadrature method and its application to solve two-dimensional incompressible Navier-Stokes equations. Comput. Methods Appl. Mech. Eng. 192, 941-954 (2003) https://doi.org/10.1016/S0045-7825(02)00618-7

[33] S. Quan, Local RBF-based differential quadrature collocation method for the boundary layer problems. Eng. Anal. Boundary Elem. 34(3), 213-228 (2010) https://doi.org/10.1016/j.enganabound.2009.10.004

[34] J.-S. Chen, L. Wang, H.-Y. Hu, S.-W. Chi, Subdomain radial basis collocation method for heterogeneous media. Int. J. Numer. Meth. Eng. 80(2), 163-190 (2009) https://doi.org/10.1002/nme.2624

[35] N. Mai-Duy, T. Tran-Cong, Compact local integrated-RBF approximations for second-order elliptic differential problems. J. Comput. Phys. 230(12), 4772-4794 (2011) https://doi.org/10.1016/j.jcp.2011.03.002

[36] R.H. Chen, Z.M. Wu, Solving hyperbolic conservation laws using multiquadric quasi interpolation. Numer. Methods Partial Differ. Eq. 22(4), 776-796 (2006) https://doi.org/10.1002/num.20115

[37] Bhatia, G. S., & Arora, G. (2016). Radial basis function methods for solving partial differential equations-a review. Indian Journal of Science and Technology, 9(45), 1-18. https://doi.org/10.17485/ijst/2016/v9i45/105079

[38] Patel, V. G., & Rachchh, N. V. (2020). Meshless method-review on recent developments. Materials today: proceedings, 26, 1598-1603 https://doi.org/10.1016/j.matpr.2020.02.328

[39] A. I. Tolstykh, On using RBF-based differencing formulas for unstructured and mixed structured-unstructured grid calculations, in Proceedings of the 16th IMACS World Congress 228 (Lausanne, 2000), 4606-4624.

[40] A point interpolation meshless method based on radial basis functions,Int.J.Numer. Methods Engrg. 54 (2002), 1623-1648. https://doi.org/10.1002/nme.489

[41] Fornberg, B., & Flyer, N. (2015). A primer on radial basis functions with applications to the geosciences. Society for Industrial and Applied Mathematics https://doi.org/10.1137/1.9781611974041

[42] Milne. (1953). Numerical solution of differential equations. Wiley, New York.

[43] Lambert, J. D. (1973). Computational methods in ordinary differential equations. Introductory mathematics for scientists and engineers. Wiley, New York.

[44] Singla, R., Singh, G., Ramos, H., & Kanwar, V. (2023). An efficient optimized adaptive step-size hybrid block method for integrating w″ = f (t, w, w′) directly. Journal of Computational and Applied Mathematics, 420, 114838. https://doi.org/10.1016/j.cam.2022.114838

[45] Omar, Z., & Adeyeye, O. (2016). k-Step block method algorithm for arbitrary order ordinary differential equations. International Journal of Mathematical Analysis, https://doi.org/10.12988/ijma.2016.614

[46] Ngwane, F. F., & Jator, S. N. (2014). L-Stable Block Hybrid Second Derivative Algorithm for Parabolic Partial Differential Equations. American Journal of Computational Mathematics, 04(02), 87-92. https://doi.org/10.4236/ajcm.2014.42008

[47] Olaiya, O. O., Azeez, R. A., & Modebei, M. I. (2021). Efficient Hybrid Block Method For The Numerical Solution Of Second-order Partial Differential Problems via the Method of Lines. Journal of the Nigerian Society of Physical Sciences, 26-37. https://doi.org/10.46481/jnsps.2021.140

[48] Rufai, M. A., & Carpentieri, B. (2023). A variable step-size implementation of a new one-step block method for integrating Burgers' model equation. Alexandria Engineering Journal, 83, 355-366. https://doi.org/10.1016/j.aej.2023.09.078

[49] Mehta, A., Singh, G., & Ramos, H. (2023). Numerical solution of time dependent nonlinear partial differential equations using a novel block method coupled with compact finite difference schemes. Computational and Applied Mathematics, 42(4). https://doi.org/10.1007/s40314-023-02345-3

[50] Gu, Y. T., & Liu, G. R. (2005). A meshfree weak-strong (MWS) form method for time dependent problems. Computational Mechanics, 35(2), 134-145. https://doi.org/10.1007/s00466-004-0610-0

[51] Kaur, Anurag, V. Kanwar, and Higinio Ramos. "An optimized algorithm for numerical solution of coupled Burgers equations." Applied Numerical Mathematics 204 (2024): 352-361 https://doi.org/10.1016/j.apnum.2024.06.019

[52] Shin, S., Sommer, M., Reich, S., & Névir, P. (2010). Evaluation of three spatial discretization schemes with the Galewsky et al. test. Atmospheric Science Letters, 11(3), 223-228. https://doi.org/10.1002/asl.279

[53] Tsai, A. Y. J., Chan, R. P. K., & Wang, S. (2014). Two-derivative Runge-Kutta methods for PDEs using a novel discretization approach. Numerical Algorithms, 65(3), 687-703. https://doi.org/10.1007/s11075-014-9823-2

[54] Le Borne, S., & Leinen, W. (2023). Guidelines for RBF-FD discretization: Numerical experiments on the interplay of a multitude of parameter choices. Journal of scientific computing, 95(1), 8. https://doi.org/10.1007/s10915-023-02123-7

[55] Arora, G., KiranBala, Emadifar, H., & Khademi, M. (2023). A review of radial basis function with applications explored. Journal of the Egyptian Mathematical Society, 31(1), 6. https://doi.org/10.1186/s42787-023-00164-3

[56] Ng, Y. L., Ng, K. C., & Sheu, T. W. H. (2019). A new higher-order RBF-FD scheme with optimal variable shape parameter for partial differential equation. Numerical Heat Transfer, Part B: Fundamentals, 75(5), 289-311. https://doi.org/10.1080/10407790.2019.1627811

[57] Mojarrad, F. N., Veiga, M. H., Hesthaven, J. S., & Öffner, P. (2023). A new variable shape parameter strategy for RBF approximation using neural networks. Computers & Mathematics with Applications, 143, 151-168. https://doi.org/10.1016/j.camwa.2023.05.005

[58] Li, Yang, Dejun Liu, Zhexu Yin, Yun Chen, and Jin Meng. “Adaptive selection strategy of shape parameters for LRBF for solving partial differential equations.” Applied Mathematics and Computation 440 (2023): 127645. https://doi.org/10.1016/j.amc.2022.127645

[59] Robert Schaback, Error estimates and condition numbers for radial basis function interpolation, Adv. Comput. Math. 3 (3) (1995) 251-264 https://doi.org/10.1007/BF02432002

[60] Bengt Fornberg, Cécile Piret, On choosing a radial basis function and a shape parameter when solving a convective PDE on a sphere, J. Comput. Phys. 227 (5) (2008) 2758-2780. https://doi.org/10.1016/j.jcp.2007.11.016

[61] Rolland L. Hardy, Multiquadric equations of topography and other irregular surfaces, J. Geophys. Res. (1896-1977) 76 (8) (1971) 1905-1915 https://doi.org/10.1029/JB076i008p01905

[62] Richard Franke, Scattered data interpolation: tests of some methods, Math. Comput. 38 (1982) 181-200. https://doi.org/10.1090/S0025-5718-1982-0637296-4

[63] G. Wahba, Spline Models for Observational Data, Society for Industrial and Applied Mathematics, 1990 https://doi.org/10.1137/1.9781611970128

[64] R.E. Carlson, T.A. Foley, The parameter R2 in multi-quadric interpolation, Comput. Math. Appl. 21 (9) (1991) 29-42. https://doi.org/10.1016/0898-1221(91)90123-L

[65] M.L. Stein, Interpolation of Spatial Data: Some Theory for Kriging, Springer, 1999. https://doi.org/10.1007/978-1-4612-1494-6

[66] F. Afiatdoust, M. Esmaeilbeigi, Optimal variable shape parameters using genetic algorithm for radial basis function approximation, Ain Shams Eng. J. 6 (2) (2015) 639-647 https://doi.org/10.1016/j.asej.2014.10.019

[67] J. Biazar, M. Hosami, Selection of an interval for variable shape parameter in approximation by radial basis functions, Adv. Numerical Anal. (2016) https://doi.org/10.1155/2016/1397849

[68] Biazar, J., & Hosami, M. (2017). An interval for the shape parameter in radial basis function approximation. Applied Mathematics and Computation, 315, 131-149. https://doi.org/10.1016/j.amc.2017.07.047

[69] Koupaei, J. A., Firouznia, M., & Hosseini, S. M. M. (2018). Finding a good shape parameter of RBF to solve PDEs based on the particle swarm optimization algorithm. Alexandria engineering journal, 57(4), 3641-3652. https://doi.org/10.1016/j.aej.2017.11.024

[70] Michael Mongillo, Choosing basis functions and shape parameters for radial basis function methods, SIAM Undergrad. Res. Online 4 (190-209) (2011) 2-6. https://doi.org/10.1137/11S010840

[71] Oleg Davydov, Dang Thi Oanh, On the optimal shape parameter for Gaussian radial basis function finite difference approximation of the Poisson equation, Comput. Math. Appl. 62 (5) (2011) 2143-2161. https://doi.org/10.1016/j.camwa.2011.06.037

[72] Bengt Fornberg, Grady Wright, Stable computation of multiquadric interpolants for all values of the shape parameter, Comput. Math. Appl. 48 (5-6) (2004) 853-867. https://doi.org/10.1016/j.camwa.2003.08.010

[73] Grady B. Wright, Bengt Fornberg, Stable computations with flat radial basis functions using vector-valued rational approximations, J. Comput. Phys. 331 (2017) 137-156. https://doi.org/10.1016/j.jcp.2016.11.030

[74] Ramos, Higinio, and Paul Popescu. “How many k-step linear block methods exist and which of them is the most efficient and simplest one?.” Applied Mathematics and Computation 316 (2018): 296-309. https://doi.org/10.1016/j.amc.2017.08.036

[75] Ramos, Higinio. “An optimized two-step hybrid block method for solving rst-order initial-value problems in ODEs.” Differential Geometry-Dynamical Systems 19 (2017).

[76] Mehta, A., Singh, G., & Ramos, H. (2025). Efficient solution of one-dimensional time-dependent partial differential equations using a multi-step block method combined with compact finite difference schemes. Computational and Applied Mathematics, 44(5), 261. https://doi.org/10.1007/s40314-025-03219-6

[77] Mittal RC, Rohila R (2018) Traveling and shock wave simulations in a viscous Burgers’ equation with periodic boundary conditions, Int. J. Appl. Comput. Math. 4 (150). https://doi.org/10.1007/s40819-018-0582-y

[78] Mohanty, R. K., Weizhong Dai, and Fei Han. “Compact operator method of accuracy two in time and four in space for the numerical solution of coupled viscous Burgers’ equations.” Applied Mathematics and Computation 256 (2015): 381-393. https://doi.org/10.1016/j.amc.2015.01.051

[79] Bak, Soyoon, and Yonghyeon Jeon. “Algorithms for coupled Burgers’ equations by sharing characteristic curves within BSLM.” Advances in Continuous and Discrete Models 2023, no. 1 (2023): 39. https://doi.org/10.1186/s13662-023-03785-1

[80] A. Ba¸ shan, A numerical treatment of the coupled viscous Burgers’ equation in the presence of very large Reynolds number, Phys. A, Stat. Mech. Appl. 545 (2020) 123755. https://doi.org/10.1016/j.physa.2019.12375